

Article

# Synthesis and Characterization of Te Nanotubes Decorated with Pt Nanoparticles for a Fuel Cell Anode/Cathode Working at a Neutral pH

Maria Rachele Guascito <sup>1,\*</sup> , Daniela Chirizzi <sup>2</sup>, Emanuela Filippo <sup>3</sup>, Francesco Milano <sup>4</sup>  and Antonio Tepore <sup>3</sup>

<sup>1</sup> Dipartimento di Scienze e Tecnologie Biologiche e Ambientali, Università del Salento, S.P. Lecce-Monteroni, 73100 Lecce, Italy

<sup>2</sup> Istituto Zooprofilattico Sperimentale di Puglia e Basilicata, Via Manfredonia 20, 71121 Foggia, Italy; daniela.chirizzi@izspb.it

<sup>3</sup> Dipartimento di Beni Culturali, Università del Salento, S.P. Lecce-Monteroni, 73100 Lecce, Italy; filippo.emanuela@libero.it (E.F.); antonio.tepore@unisalento.it (A.T.)

<sup>4</sup> Istituto di Scienze delle produzioni Alimentari, Consiglio Nazionale delle Ricerche, S.P. Lecce-Monteroni, 73100 Lecce, Italy; francesco.milano@cnr.it

\* Correspondence: maria.rachele.guascito@unisalento.it; Tel.: +39-0832-299453

Received: 7 March 2019; Accepted: 24 March 2019; Published: 3 April 2019



**Abstract:** In fuel-cell technology development, one of the most important objectives is to minimize the amount of Pt, the most employed material as an oxygen reduction and methanol oxidation electro-catalyst. In this paper, we report the synthesis and characterization of Te nanotubes (TeNTs) decorated with Pt nanoparticles, readily prepared from stirred aqueous solutions of PtCl<sub>2</sub> containing a suspension of TeNTs, and ethanol acting as a reducing agent, avoiding the use of any hydrophobic surfactants such as capping stabilizing substance. The obtained TeNTs decorated with Pt nanoparticles (TeNTs/PtNPs) have been fully characterized by X-ray diffraction (XRD), transmission electron microscopy (TEM), selected area diffraction patterns (SAD), X-ray photoelectron spectroscopy (XPS), and cyclic voltammetry (CV). We demonstrated that the new material can be successfully employed in fuel cells, either as an anodic (for methanol oxidation reaction) or a cathodic (for oxygen reduction reaction) electrode, with high efficiency in terms of related mass activities and on-set improvement. Remarkably, the cell operates in aqueous electrolyte buffered at pH 7.0, thus, avoiding acidic or alkaline conditions that might lead to, for example, Pt dissolution (at low pH), and paving the way for the development of biocompatible devices and on-chip fuel cells.

**Keywords:** Te nanotubes decorated with Pt nanoparticles; fuel cell neutral pH; oxygen reduction reaction; methanol oxidation reaction; X-ray photoelectron spectroscopy

## 1. Introduction

Nanomaterials have become of paramount importance as advanced systems in numerous fields of research and technological applications, mainly due to the high opportunity to finely tune the properties of the material, by changing their dimensions [1]. In addition, nanomaterials with anisotropic shapes are characterized by a higher surface area and several contact points (borders, inner or outer surfaces) that can be functionalized in numerous ways [2], if compared to the isotropic counterpart. In this context, carbon nanotubes and nanowires represented a breakthrough in the nano-science research in developing 1D anisotropic nanoparticles, since their discovery in 1991 [3].

In electrocatalytic applications, the selection of the optimal electrode materials, to make anodes/cathodes suitable to develop advanced fuel cells or electrochemical detectors, is influenced

for the most part by their surface chemical composition and physical properties, because the electro-oxidation/reduction rate of the electroactive substances severely depends on these parameters. In the last three decades, to enhance the electrochemical processes in these devices, there has been an increasing interest to develop new innovative anisotropic nanomaterials in different shapes and sizes, to make chemically modified electrodes (CMEs), based on metal or multi-metallic nanostructures, thanks to their extraordinary electrocatalytic activity decreasing the over-potentials of many substances, with respect to common unmodified electrodes [4]. Accordingly, almost since 1980, a variety of techniques and treatments have been developed that are useful to modify the surface of the classical electrodes to obtain specific electrocatalytic properties, by using either mono- or multi-metallic nanostructures [5]. Multi-metallic structures, either in form of alloy or nano-sized core-shell, show special characteristics like superior optical, catalytic, electronic, and magnetic properties, which are directly dependent on their chemical composition, their nanometric dimensions are typically superior to their pure element counterparts, as well [6]. However, even if most studies on the synthesis of alloy or core-shell nanostructures have been particularly devoted to developing isotropic spherical structures, methods for making alloy or core-shell structures with different anisotropic shapes, like nanowires, nanotubes etc., have also been reported [7–9].

In this context, the platinum material has been extensively investigated and studied for its potential in technological applications, including catalysis in many chemical reactions and as an electrode material, in fuel cells or electrochemical sensors development. On the other hand, massive application of the expensive Pt-based catalyst implies a substantial increase in actual costs in fuel cells or sensor technology development, thereby, reducing their commercial competitiveness. To reduce the effective device cost by improving the electrocatalytic efficiency of electrode materials with the increment of the active surface, the use of platinum nanostructures in different suitable shapes (i.e., nanowires, nanotubes, nanoparticles) has been studied [10–15]. Additionally, the presence of a different metal (e.g., Cu, Sn, Co, Ni, Pd, Au, Ag, Fe, Zn, Ru) to form platinum-based hetero-nanostructures or alloy catalysts, can further reduce the Pt amount to be used, since these alloys exhibit better electrocatalytic properties than platinum monometallic counterpart nanomaterials [16]. This strategy is particularly helpful when Pt is used in combination with other inexpensive metals. Accordingly, studies have been focused on the synthesis and characterization of new nanostructured materials based on Pt, in different shapes like nanowires and nanoparticles, and, more recently, hollow structured nanomaterials (i.e., nanotubes, nanocages, hollow nanospheres) to make bimetallic or multi-metallic nanostructures, [6,17] operating in most cases in acidic or alkaline environment. However, considering that in an acidic environment Pt can be dissolved, negatively affecting fuel cell and electrochemical sensor-related performance, the use of neutral pH is desirable, as it makes this detrimental effect less favorable [18]. In addition, in carbonaceous abiotic membrane-free fuel cells, the use of electrolytic solution at pH 7.0 (near the buffering point of bicarbonate/CO<sub>2</sub>), has recently been reported as a valid alternative to alkaline conditions in which the adsorption of CO<sub>2</sub>, produced by carbonaceous electro-oxidation in the electrolyte, results in a pH decrease that induces instability in the performance of the alkaline direct methanol fuel cell (DMFC) [19,20]. Finally, metal alloy materials (i.e., platinum-based), used either as anode or cathode, in fuel cell systems working at a neutral pH, can be applied in the development of advanced devices such as (bio-)fuel, micro-fuel, and on-chip fuel cells [20–23].

Pt electrodes modified with Te micro- and nanostructures have been proven to have a higher activity than pure Pt bulk for ethanol and glucose electro-oxidation, and H<sub>2</sub>O<sub>2</sub> electro-reduction, making them an important material for the improvement of carbonaceous fuel cells (i.e., direct alcohol fuel cells, DAFCs) [24] and as enzyme-less glucose and H<sub>2</sub>O<sub>2</sub> sensors [25,26], which are also able to operate with high efficiency under a safe neutral pH environment.

In this work we reported a study on the synthesis and characterization of Te nanotubes decorated with Pt nanoparticles, having an equimolar Pt/Te ratio, readily prepared from aqueous solutions of  $\text{PtCl}_2$  containing Te nanotube (TeNTs) mixtures, with ethanol present as a reducing agent, in a stirred bath, without using any hydrophobic surfactant as a capping and stabilizing agent. We demonstrated that the fully characterized new material is suitable to be efficiently used in direct fuel cell devices, either as an anodic and cathodic material working in neutral pH conditions to develop safe and bio-compatible devices for both the oxygen reduction reaction (ORR) and the methanol oxidation reaction (MOR), kinetically competitive with respect to acidic or alkaline electrolytic unsafe conditions.

## 2. Results

The Te nanotubes used in this work were directly prepared by exploiting their natural tendency to form this kind of structure, when the Te powder is heated at 400 °C, under Ar atmosphere—at this temperature the Te atoms evaporated and condensed, forming nanotubes [27]. Scanning electron microscope images (Figure 1) and X-ray diffraction patterns showed that the as-synthesized Te had a nanotubular single-crystalline morphology, with a hexagonal cross-section. Te nanotubes were typically 0.5–6 mm in length and 150–450 nm in external diameter. For the nanotube decoration with Pt nanoparticles, an ethanolic suspension of these TeNTs was subsequently mixed with an aqueous solution of  $\text{PtCl}_2$ . By heating the solution, the reduction of Pt on behalf of ethanol was promoted and it formed Pt(0) deposits on the TeNT surface as nanoclusters. The relative amounts of TeNT and  $\text{PtCl}_2$ , temperature and reaction time were optimized, in order to obtain structures containing equimolar fractions of Pt and Te. The TeNTs/PtNPs nanostructures were used to modify the glassy carbon (GC) electrode, by simply drop casting an ethanolic suspension of decorated nanotubes onto the electrode surface. After solvent evaporation, the nanostructured film was stabilized by various cyclic voltammetry cycles, until a steady state current was obtained and activated in  $\text{H}_2\text{SO}_4$  0.5 M, as is usual for Pt electrodes. The modified GC electrodes were finally used for electrocatalytic methanol oxidation and  $\text{O}_2$  reduction experiments, respectively.

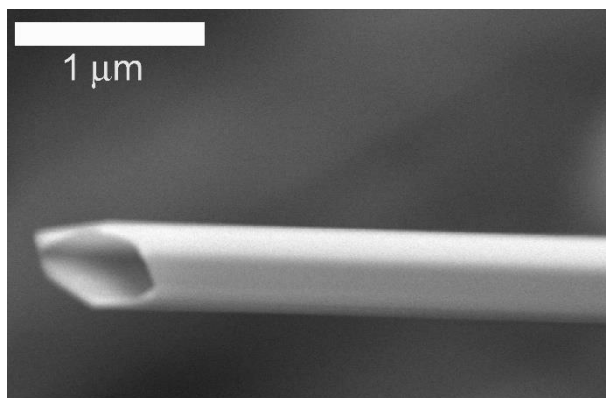


**Figure 1.** Typical SEM image of a single Te nanotube (TeNT).

### 2.1. Morphological and Spectroscopic Characterization

The X-ray diffraction (XRD) pattern of TeNTs/PtNPs composite samples in Figure 2 shows that the stronger and sharper peaks can be indexed according to the hexagonal crystal structure of tellurium [JCPDS No 36-1452], with a lattice constant of  $a = 0.44579$  nm and  $c = 0.59270$  nm. Along with the reflection peaks corresponding to Te, a number of lines were found to coincide with the (111), (200), and (220) planes of the face-centered cubic (fcc) platinum structure, with a lattice constant  $a = 0.39231$  nm [JCPDS no. 04-0802]. These observations suggested that both Te and Pt were well crystallized nanostructures.

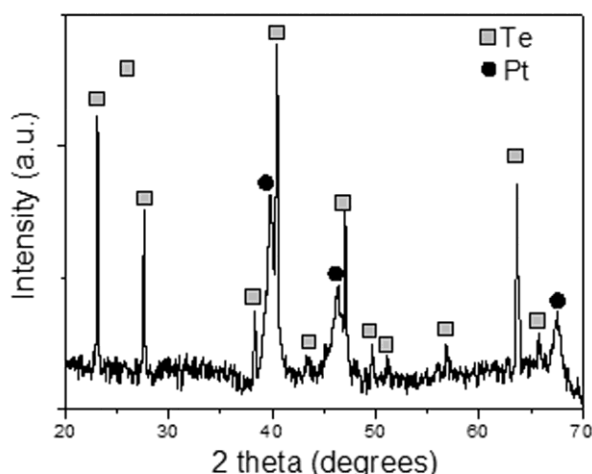


**Figure 2.** XRD pattern of Te nanotubes/Pt nanoparticles (TeNTs/PtNPs) composite nanostructures.

Figure 3b shows a representative transmission electron microscopy (TEM) image of straight tellurium nanotubes decorated with Pt nanoparticles. The nanotubes exhibited a tubular morphology with open prongs at the end and a mean diameter in the range of 150–450 nm. TEM observations also revealed the presence of abundant nanoparticles, decorating the external surface of the nanotubes, with a diameter in the range 50–200 nm. The selected area diffraction pattern acquired on the extreme tip of the nanotube (Figure 3a) evidenced that the tubes grew along the [001] direction, in agreement with the preferred growth direction observed in our previous work [27]. The selected area diffraction pattern recorded on the nanoparticles assembly shown in Figure 3c, clearly exhibited diffraction rings with  $d$  spacing, which could be indexed according to the fcc structure of Pt. In fact, the concentric rings could be assigned as diffraction from the {111}, {200}, {220}, {311}, and {222} planes, starting from the centermost ring.

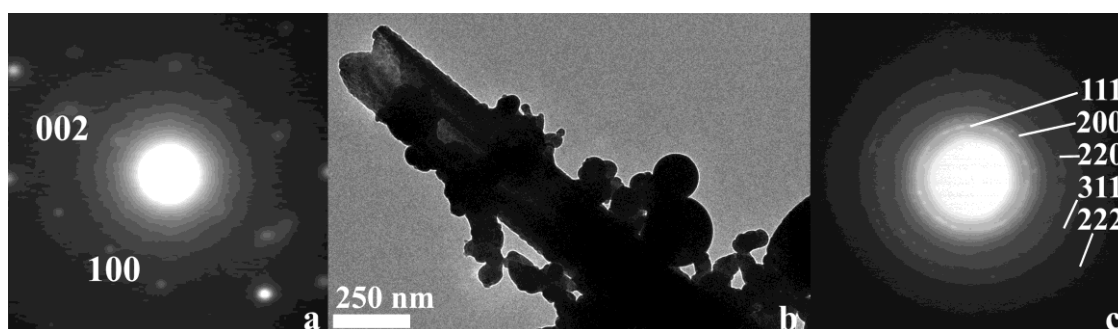


**Figure 3.** Typical TEM image of the TeNTs/PtNPs composite nanostructures (b), along with the selected area diffraction pattern recorded from the extreme tip of the nanotube (a), and nanoparticles assembly (c).

These results confirmed that the synthesized products were composed of Te nanotubes decorated with Pt nanoparticles.

XPS analysis was carried out on the TeNTs/PtNPs samples. As expected, the survey spectra of TeNTs/PtNPs samples showed the most intense Pt4f and Pt4d photopeak signals from the platinum top-layer nanoparticles, in addition to the O1s, C1s, Te3d, Te4d, and the Te (M4N45N45) base signals. C1s peak signals were attributed to carbon-containing species present as structure contaminations, while O peak signals could be attributed, both to carbonaceous contamination (O1s peak component at  $532.5 \pm 0.1$  eV, National Institute of Standards and Technology (NIST), and Te/Pt oxidized species coming from the top layer of the samples (O1s peak component at  $530.7 \pm 0.1$  eV, NIST), data not shown. The high resolution (HR) regions of Te3d and Pt5f were employed to investigate the TeNTs/PtNPs surface chemical speciation and composition. Figure 4A shows the main peak pair Te3d<sub>5/2</sub> and

Te3d<sub>3/2</sub>. To fit Te3d<sub>5/2</sub> and Te3d<sub>3/2</sub> HR region, typically three peak pair components were employed. According to literature data [28,29], the peak pair at lower BE (572.8 ± 0.1 eV and 583.2 ± 0.1 eV) was attributed to Te(0). Instead, while the peak pair component at higher BE (576.0 ± 0.1 eV and 586.4 ± 0.1 eV) was associated to Te (IV) oxide of the surface (TeO<sub>2</sub>), the peak pair at 574.1 ± 0.1 eV and 584.5 ± 0.1 eV was attributed to the Te–Pt interacting phase [28]. The calculated tellurium atomic relative percentage (At. %) was 65% of Te(0), 25% of Te(IV), and 10% of Te–Pt. Typically three peak pair components were also used to fit Pt4f<sub>7/2</sub> and Pt4f<sub>5/2</sub> HR region (Figure 4B). The most intense peak pair was Pt(0) at 71.3 ± 0.1 eV and 74.1 ± 0.1 eV (NIST) (At. % 73), the second peak pair (72.3 ± 0.1 eV and 75.7 ± 0.1 eV) was the Pt–Te interacting phase (i.e., platinum nucleation sites inter-phase) (At. % 23). The last peak pair at 73.2 ± 0.1 eV and 76.9 ± 0.1 eV, in accordance with the NIST data and the measured PtCl<sub>2</sub> standard (Pt4f<sub>7/2</sub> 73.5 ± 0.1 eV) was attributed to the PtCl<sub>2</sub> present as traces and coming from the synthesis process, considering also the concomitant presence of Cl2p peak signal in the survey spectrum. XPS Pt/Te elemental ratio was estimated to be about 1.4, confirming the platinum surface enrichment of tellurium nanotubes, in accordance with the TEM results.

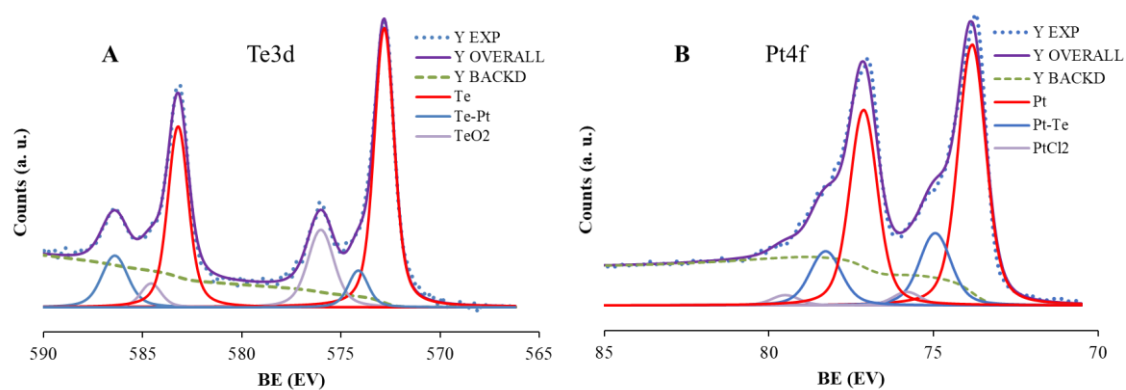


**Figure 4.** High Resolution (HR) Te3d (A) and Pt4f (B) XPS peaks related to the TeNT/PtNP composite nanostructures.

In our experiments, the outer surface of the Te nanotubes served as a substrate for the nucleation and growth of Pt nanoparticles. PtCl<sub>2</sub> was reduced by ethanol to form Pt nanoparticles, which will attach on the surface of the Te nanotubes. It is reasonable to suppose that, like what happens in the case of the coating of selenium nanowires with Pt [30], two distinct reduction reaction patterns occurred—an initial reduction of Pt(II) salt by the Te template, itself, at the interface, promoting the Pt nucleation process, in accord with the presence of the characteristic Pt–Te interacting species (i.e., XPS experiments) and the reduction of the Pt(II) salt by the alcohol reagent that now promotes the growth of the Pt nucleation sites. The galvanic reduction of the Pt(II) by the Te template caused the formation of some nucleation sites for the Pt nanoparticles formation, randomly distributed along the nanotubes and detected by XPS, due to its high surface sensibility. As the reaction proceeded, Pt(II) salt reduction by alcohol became dominant, causing a gradual growth of the nanoparticles decorating the nanotubes and, at the same time, causing the formation of nanoparticles in the solution. The latter ones could attach to the outer surface of the Te nanotubes or to the Pt nanoparticles, randomly formed on them.

## 2.2. Electrochemical Characterization of the TeNT/PtNP Materials onto the GC Electrodes

Cyclic voltammetric experiments were used to study the main electrochemical properties of bimetallic composite TeNTs/PtNPs materials cast onto GC disk electrodes in a phosphate buffer (pH 7.0) (Figure 5). In a direct scan (oxidation) two peaks were observed, respectively, at +285 mV and at +520 mV, attributed to the Te(0)/Te(IV) and Pt(0)/Pt(II) processes also associated with the O<sub>2</sub> monolayer adsorption [28,31]. In a reverse scan, the peak observed in reduction at +100 mV was ascribed to the Te(IV)/Te(0) and the Pt(II)/Pt(0) overlapped peaks, which involved the species formed/adsorbed in oxidation scans [28]. This was in accordance with the parallel increase of related

currents, in oxidation and reduction, observed in the potential range between  $-100$  mV and  $+800$  mV. The peak at  $-276$  mV can be tentatively attributed to the reduction processes of the Te and Pt sites (i.e., different Te/Pt sites on anisotropic nanotube shapes), requiring higher overpotentials. However, since the overall currents increase with cycling, particularly in the region of the Pt/Te reduction zone between  $-200$  mV and  $+200$  mV [28], the potential scan probably restructured the Pt and Te atoms surface distribution, due to the dissolution/re-deposition of different Te and Pt species, as function of the voltammetric cycle numbers, accounting for the rise of the peak during the reduction, at  $+150$  mV, a potential closer to the value of  $+50$  mV was already observed on the Pt–Te similar bimetallic system and correlated principally to the Pt species reduction [28]. The measured  $\text{PtO}_2$  reduction peak in the same conditions on bare Pt was at  $+50$  mV [32]. Moreover, a steady-state current, corresponding to a stable surface composition, was typically reached after about 30 CV cycles, necessary to obtain the suitable TeNTs/PtNPs/GC modified electrodes.

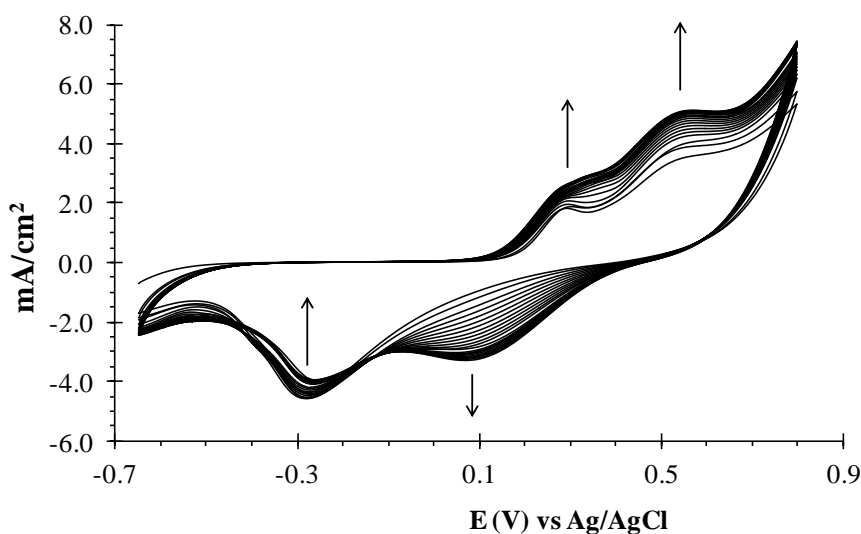


**Figure 5.** Characterization of TeNT/PtNP materials onto the GC electrodes by cyclic voltammetry in phosphate buffer, pH 7.0. Scan rate  $50 \text{ mV s}^{-1}$ . Upward and downward arrows indicate the current change in the subsequent cyclic voltammetry (CV) scans.

The prepared TeNTs/PtNPs/GC electrodes were electrochemically activated in the  $\text{H}_2\text{SO}_4$  0.5 M, before using in methanol electro-catalysis in neutral pH experiments, since preliminary tests suggested that a significant increase of the catalytic currents were reached after these pre-treatments. The CV results reported in Figure 6 compared the typical voltammograms recorded onto the clean GC (curve a) and Pt (curve b) conventional electrodes, as controls, and onto the TeNTs/PtNPs/GC modified electrodes, in a clean phosphate buffer solution. All CV curves were obtained at a scan rate of  $50 \text{ mVs}^{-1}$ , in the potential range between  $-650$  mV and  $+800$  mV. As expected, conventional bare GC electrode did not show any specific electrochemical activity (Figure 6, curve a and related inset). Instead an evident electrochemical activity was recorded, both, on the conventional bare Pt electrode (curve b) and the TeNTs/PtNPs/GC modified electrode (curve c). Characteristic peaks due to the atomic hydrogen adsorption and desorption on the platinum active sites were observed in the cathodic “hydrogen region” in the neutral pH electrolytes, between  $-650$  mV and  $-200$  mV vs. Ag/AgCl [33,34], either on the bare Pt or the TeNTs/PtNPs/GC-modified electrodes. Therefore, by modifying the electrochemically inert GC electrode surface with the TeNTs/PtNPs nanostructures, the electrochemical hydrogen adsorption/desorption processes could be activated as typically observed on bare platinum in the potential range between  $-520$  mV and  $-220$  mV, at a neutral pH, after activating it in  $\text{H}_2\text{SO}_4$  0.5 M. In addition, besides the intense activity in the “hydrogen region”, TeNTs/PtNPs/GC-modified electrodes in oxidation, showed a good stable peak at  $E_{\text{pa}} = +500$  mV, with a peak in the reverse scan at  $E_{\text{pc}} = +150$  mV being attributed to both Pt(0)/Pt(II) and Te(0)/Te(IV) but not well-resolved red-ox

processes-related peaks. Otherwise, the shoulder at  $-140$  mV has been attributed principally to the Te(IV)/Te(0) reduction process [26]. In detail, the charge amount ( $Q_H$ ) exchanged during hydrogen desorption on TeNTs/PtNPs/GC, was almost  $4 \text{ mC cm}^{-2}$  in the actual experimental conditions. Correspondent electrochemically active surface area (ECSA), that can provide important information relative to the number of Pt sites that are catalytically actively available for an electrochemical reaction [32], was estimated to be  $20 \text{ m}^2/\text{g}_{\text{Pt}}$ , by the following equation [12]:

$$\text{ECSA} = Q_H / (q_H \times m_{\text{Pt}})$$

where  $Q_H$  is the charge amount exchanged during hydrogen desorption on Pt nano-particle sites in the “hydrogen region”,  $q_H = 210 \text{ } \mu\text{C cm}^{-2}$  is the charge required to oxidize a monolayer of  $\text{H}_2$  on the Pt surface and  $m_{\text{Pt}} = 7 \text{ } \mu\text{g}$  is the amount of platinum loaded on the electrode. This value has been estimated by considering the amount of Pt/Te composite solution cast on the electrodes and corrected by taking into account the efficiency of the TeNTs/PtNPs deposition obtained by the  $Q_{\text{TeNT/PtNP(ox)}}/Q_{\text{TeNT/PtNP/GC(ox)}}$  ratio, estimated at almost 3:1, where,  $Q_{\text{TeNT/PtNP(ox)}}$  has been obtained considering the overall charge quantities related to the platinum/tellurium oxidation measured in the steady-state condition (Figure 5, last cycle).  $Q_{\text{TeNT/PtNP/GC(ox)}}$  is the overall charge related to the platinum/tellurium oxidation of the same modified electrodes obtained in the phosphate buffer, after their activation in  $\text{H}_2\text{SO}_4$  0.5 M (Figure 6, curve c).

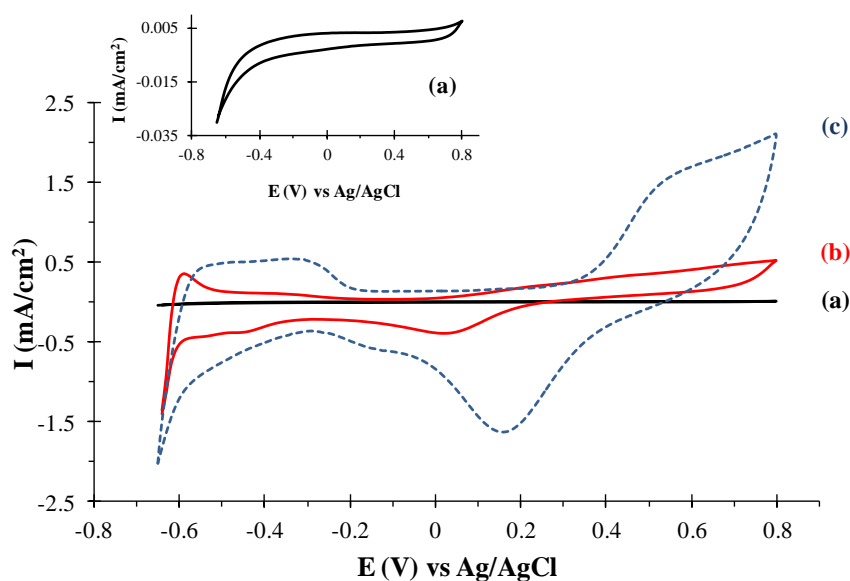


**Figure 6.** Characterization of GC (curve a), bare Pt (curve b) and TeNT/PtNP/GC (curve c) electrodes by Cyclic Voltammetry in phosphate buffer, pH 7.0. Scan rate  $50 \text{ mV s}^{-1}$ .

### 2.3. Electrochemical Characterization of TeNT/PtNP/GC Modified electrodes with Respect to Methanol Oxidation

The electrocatalytic activity of the as-obtained modified electrodes for the methanol oxidation reaction (MOR) was studied in phosphate buffer at pH 7.0, a neutral safe medium, by cyclic voltammetry at 100, 500, and 1000 mM methanol, respectively. Related voltammograms are shown in Figure 7A–C (green traces) and compared to the bare GC (red traces) and bare Pt (blue traces) electrodes as obtained and in Figure S1, after a subtraction of the relative background. For a direct comparison of the principal properties of the three different electrodes, anodic peak currents ( $I_{\text{pa}}$ ) and related anodic peak potentials ( $E_{\text{pa}}$ ) are reported in Table 1. Conventional GC electrode, as expected, was totally inactive with respect to methanol oxidation with current density levels ranging between  $-30$  and  $10 \text{ } \mu\text{Acm}^{-2}$ , with no peak current observation after methanol addition. Otherwise, bare Pt

electrodes present peaks in oxidation and reduction, related to the electrochemical activity involving the different oxidation states of platinum, showing a typical electrocatalytic activity toward methanol oxidation in the potential range between 0.00 mV and +600 mV, and a maximum of current density at around +370 mV vs. Ag/AgCl, according to the reported values at platinum electrodes in neutral pH vs. small molecular weight alcohol [35–37]. However, a rapid poisoning of the electrode at these high concentrations of methanol is observed. As a matter of fact, CV curves obtained at 500 mM (Figure 7B, trace Blue) and 1,000 mM (Figure 7C, trace Blue) are almost coincident, with a tendency to decrease with the increase of methanol concentration. A remarkable catalytic oxidation current density, ranging between 2.2 and 4.0  $\mu\text{Acm}^{-2}$ , for methanol, on the TeNTs/PtNPs catalyst-modified GC, was observed in a wider potential range from  $-200$  mV to  $+800$  mV. A consistent decrement of the methanol oxidation potential on-set, estimated to be almost of 150 mV, if compared to the bare Pt, was observed. The onset potential of methanol oxidation was an important factor in electrocatalytic study, because it represented the power to break the methanol C–H bonds and the effectiveness in removing off species partially oxidized adsorbed on the electrode surface, improving with the lowering of the onset potential. This observed behavior, together with the overall current density increment, and the potential range raising in the forward scan, with respect to the bare Pt, confirmed a synergic interaction between the Te and the Pt electroactive sites, which act to enhance the methanol electro-oxidation processes.

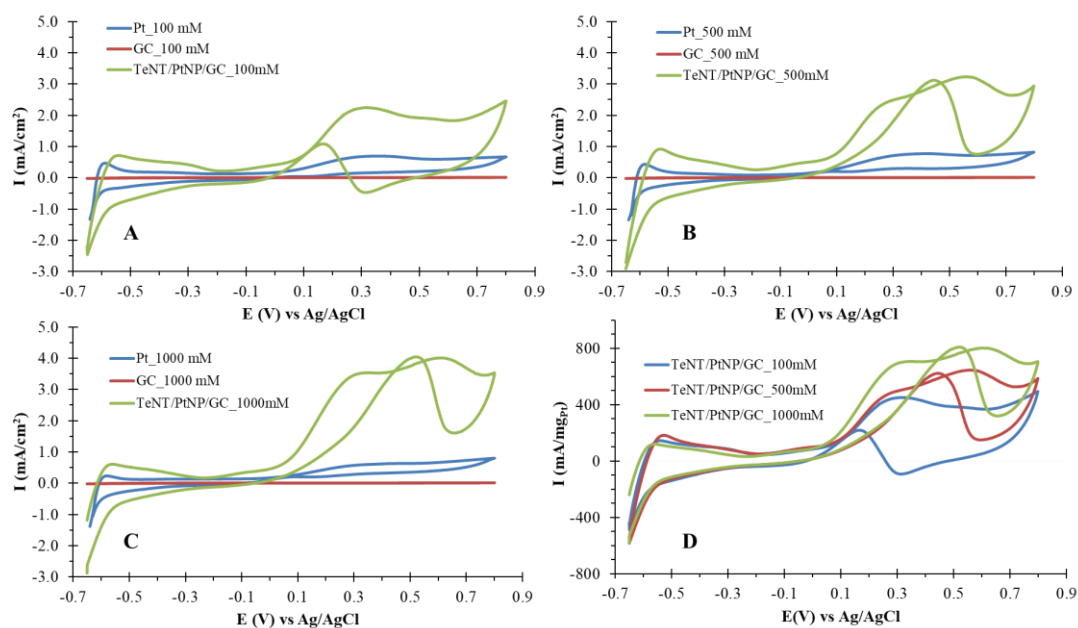


**Figure 7.** Cyclic voltammetric curves as obtained on the bare GC (red traces), bare Pt (blue traces), and TeNT/PtNP/GC (green traces) electrodes, in a phosphate buffer of pH 7.0, respectively, at 100 mM (panel (A)), 500 mM (panel (B)), and 1,000 mM (panel (C)) methanol solutions. Sweep rate  $50 \text{ mV s}^{-1}$ . The current density in panel (D) for the TeNT/PtNP/GC electrodes is normalized in reference to the real Pt surface area per mass.

Accordingly, the specific activities, measured at the corresponding higher peak potential in the forward scan, at three different methanol contents (100, 500, and 1,000 mM) were  $2.24 \text{ mA cm}^{-2}$  (at +298 mV),  $3.22 \text{ mA cm}^{-2}$  (at +547 mV), and  $4.04 \text{ mA cm}^{-2}$  (at +615 mV) respectively. Related mass activities were  $448 \text{ mA mg}_{(\text{Pt})}^{-1}$ ,  $644 \text{ mA mg}_{(\text{Pt})}^{-1}$ , and  $1615 \text{ mA mg}_{(\text{Pt})}^{-1}$ , respectively (Figure 7D). All these values were comparable or better than the recent previous data reported for the methanol electro-oxidation obtained, for example, on a highly dispersed platinum nanoparticles/carbon nitride materials in acidic media [38], on branched Pd and Pd-based trimetallic nanocrystals (NCs) with long, thin branches, and open structures operating in basic media [39], as well as on the Pt/Te bimetallic nanowires [40]. The oxidation peaks recorded in backward scan (at +160 mV, +440 mV,

and +530 mV) were attributed to the removal of incompletely oxidized carbonaceous species formed in the forward scan on Pt, Te, and Pt–Te active sites, which appear to be heavily influenced on the three different concentrations of methanol tested. A similar behavior, where different electrocatalytic sites are activated (see the different peaks involved in CV experiments, Figure 7), not observed on previous reported Pt/Te bimetallic and Pt/Pd/Te trimetallic systems in acid pH [40,41], could be attributed to the coexistence on the top of the surface of Te–Pt ad-atoms, directly involved in methanol electrocatalytic oxidation. The observed synergy plays a central role in reducing the onset, as well as the poisoning effect at potentials greater than +350 mV observed in methanol electro-oxidation on bare Pt. Accordingly, in the potential range of +350 mV to +800 mV, peak currents at +547 mV and +615 mV, rise with the methanol concentration increment. Finally, a consistently high platinum catalytic activity of the TeNT/PtNP/GC electrodes is not only confirmed but further enhanced in the “hydrogen region”, in methanol presence. The observed current density that ranges from  $-2.0$  to  $0.5 \text{ mAcm}^{-2}$ , in a phosphate buffer that is methanol-free (Figure 6), increases to a range of  $-3.0$  to  $1.0 \text{ mAcm}^{-2}$  in methanol 500 mM. A saturation effect was observed at methanol 1,000 mM (Figure 7).

**Table 1.** Comparison between anodic peak currents (I<sub>pa</sub>) and related peak potentials (E<sub>pa</sub>) obtained from CVs curves reported in Figure 7 on bare GC, bare Pt, and TeNT/PtNP/GC electrodes respectively, at different methanol concentrations.

Electrode	I <sub>pa</sub> (mAcm <sup>-2</sup> )/E <sub>pa</sub> (mV) [MeOH] 100 mM	I <sub>pa</sub> (mAcm <sup>-2</sup> )/E <sub>pa</sub> (mV) [MeOH] 500 mM	I <sub>pa</sub> (mAcm <sup>-2</sup> )/E <sub>pa</sub> (mV) [MeOH] 1000 mM
GC	-	-	-
Pt	0.58/+370	0.74/+370	0.69/+370
TeNT/PtNP/GC	2.24/+298	3.22/+547	4.04/+615

#### 2.4. Electrochemical Characterization of TeNT/PtNP/GC Modified electrodes with Respect to Oxygen Reduction

The electrocatalytic activity of the TeNT/PtNP/GC toward the reduction of oxygen was studied in static conditions and compared to bare GC and Pt electrodes, at different O<sub>2</sub> contents. Figure 8A–C shows the typical CVs of oxygen electro-reduction at bare GC (red traces), bare Pt (blue traces), and TeNT/PtNP/GC-modified GC (green traces) electrodes in a phosphate buffer solution (pH 7.0) in N<sub>2</sub>-saturated, in atmospheric O<sub>2</sub>, and saturated O<sub>2</sub> conditions. All CVs were obtained at a scan rate of  $50 \text{ mV s}^{-1}$ , in a potential range between  $-300 \text{ mV}$  and  $+300 \text{ mV}$ . Figure S2 shows the same CVs as obtained, after subtraction of the relative background. For a direct comparison, principal properties of the three different electrodes, in terms of cathodic peak currents (I<sub>pc</sub>) and related peak potentials (E<sub>pc</sub>), are reported in Table 2. As expected, GC electrodes (Figure 8A–C; red traces) are totally inert. No catalytic reduction current density increment can be observed both in atmospheric O<sub>2</sub> and O<sub>2</sub>-saturated solutions, in the potential range employed, in comparison to the N<sub>2</sub>-saturated phosphate buffer. Otherwise, conventional Pt electrodes show an increase in the typical electrochemical activity in reduction, with an increase in the oxygen content (Figure 8A–C; blue traces), even if moderate in comparison to the TeNTs/PtNPs/GC-modified electrodes. In fact, the higher current increment for oxygen reduction was observed on TeNTs/PtNPs/GC-modified electrodes at both O<sub>2</sub> tested concentrations, with respect to the N<sub>2</sub>-saturated solution (Figure 8A–C green traces). In details, on the Pt electrodes, the current density started to increase at  $0.00 \text{ mV}$ , reaching a quasi-plateau of  $-0.20 \text{ mAcm}^{-2}$ , in atmospheric O<sub>2</sub>, and at  $+50 \text{ mV}$ , reaching a quasi-plateau of  $-0.30 \text{ mAcm}^{-2}$ , in O<sub>2</sub>-saturated solutions. Remarkably, TeNTs/PtNPs/GC showed a larger density current and peak potentials in reduction, between  $+50/+150 \text{ mV}$ , with onset at  $+250 \text{ mV}$ . These values were more positive than those measured on the bare Pt characterized from a potential peak at  $-150 \text{ mV}$  and onset at  $+200 \text{ mV}$ , and was quite similar to the recently reported value on the Pt/C catalyst [42]. A more positive potential of the oxygen reduction peak indicates a higher ORR activity of the catalyst [42], demonstrating that the catalytic properties of Pt in TeNTs/PtNPs/GCE electrodes strongly depend on the tellurium component. These data indicated that the current density rise observed in the

TeNTs/PtNPs/GC, with an O<sub>2</sub> concentration increment, which was totally absent in the GC, should be attributed to the electrocatalytic oxygen reduction process on platinum nanoparticles, enhanced in the presence of tellurium species. All these collected results point out that these hybrid nanostructures have excellent electrocatalytic activity for oxygen reduction in a neutral pH, better than the previous data obtained in similar static conditions on ultrathin platinum-coated gold nanoparticle monolayer films [43], as well as on tungsten nitride supported on carbon black [44], at an acid pH, in agreement with the observation that Pt catalyst in neutral media promotes a mechanism involving direct 4e<sup>-</sup> transfer [23]. Furthermore, the nanostructures showed an electrocatalytic activity for oxygen reduction, almost twice that of the response obtained in a neutral pH, not only on the Pt/C catalyst [42], but also on the Pt-free iron/polyindole-based electrocatalysts, as recently reported [42].

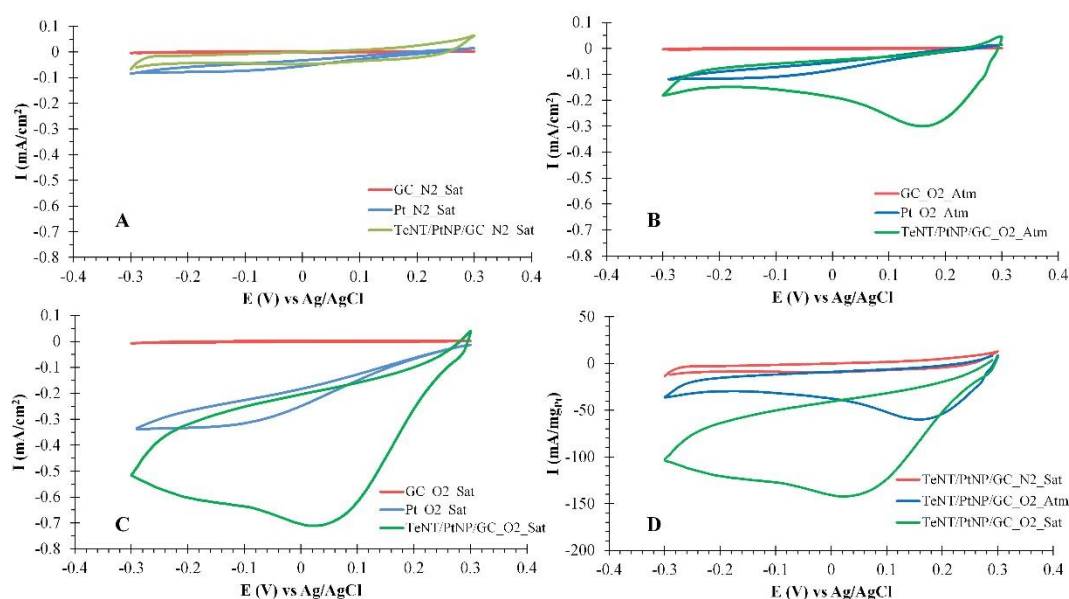


**Figure 8.** Cyclic voltammetric curves as obtained on bare GC (red traces), bare Pt (blue traces), and TeNT/PtNP/GC electrodes (green traces), in phosphate buffer pH 7.0, at N<sub>2</sub>-saturated solution (panel (A)), O<sub>2</sub> atmospheric solution (panel (B)), and O<sub>2</sub> saturated solutions (panel (C)), respectively. Sweep rate was 50 mV s<sup>-1</sup>. The current density in panel (D) for the TeNT/PtNP/GC electrodes was normalized, in reference to the real Pt surface area per mass.

**Table 2.** Comparison between the cathodic peak currents (I<sub>pc</sub>) and related peak potentials (E<sub>pc</sub>) obtained from the CVs curves, reported in Figure 8 on the bare GC, the bare Pt, and the TeNT/PtNP/GC electrodes, respectively, at different O<sub>2</sub> concentrations.

Electrode	I <sub>pc</sub> (mAcm <sup>-2</sup> )/E <sub>pc</sub> (mV)	I <sub>pc</sub> (mAcm <sup>-2</sup> )/E <sub>pc</sub> (mV)	I <sub>pc</sub> (mAcm <sup>-2</sup> )/E <sub>pc</sub> (mV)
	N <sub>2</sub> -saturated	atmospheric O <sub>2</sub>	O <sub>2</sub> -saturated
GC	-	-	-
Pt	-	-0.20/-115	-0.30/-150
TeNT/PtNP/GC	-	-0.30/+150	-0.70/+50

### 3. Materials and Methods

#### 3.1. Chemicals

Tellurium powder (≥99.9%), PtCl<sub>2</sub>, Na<sub>2</sub>HPO<sub>4</sub>, NaH<sub>2</sub>PO<sub>4</sub>, ethyl alcohol, and methanol were analytical grade reagents furnished from Sigma-Aldrich (St. Louis, MO, USA) and were used as received, with no further purification. Deionised ultra-filtered water prepared with a Milli-Q water purification system (Millipore-Merck, Milan, Italy, 18.2 MΩ cm<sup>-1</sup>) was used throughout the experiments.

### 3.2. Apparatus and Methods

All electrochemical experiments were carried out by using a  $\mu$ Stat400 DropSens (Oviedo, Spain) electrochemical potentiostat, controlled by a computer, in a conventional three-electrode cell, by means of a glassy carbon (GC) ( $A = 0.0707 \text{ cm}^2$ ) or Pt ( $A = 0.0314 \text{ cm}^2$ ) disk working electrodes, a Pt wire as a counter electrode and an Ag/AgCl, KCl (sat) as reference, in phosphate buffer solutions (pH 7.0,  $I = 0.2$ ).

X-ray diffraction (XRD), scanning electron microscopy (SEM), transmission electron microscopy (TEM), selected area diffraction patterns (SAD), and X-ray photoelectron spectroscopy (XPS) were used to characterize the chemical structure and the morphology of the as-obtained Te nanotubes, decorated with Pt nanoparticles. X-ray diffraction measurements were obtained in the reflection mode on a Mini Flex Rigaku model diffractometer, with Cu  $K\alpha$  radiation ( $\lambda = 0.154056 \text{ nm}$ ). The X-ray diffraction data were collected at a scanning rate of 0.02 degrees per second, in 2 h, ranging from  $15^\circ$  to  $80^\circ$ . Te nanotubes were carefully characterized by SEM (Tescan SEM Brno, Czech Republic), operating at 20 kV. The morphology and the crystal structure of the obtained nanostructures have been studied, using a transmission electron Hitachi H-7100 microscope (Tokyo, Japan), operating at an accelerating voltage of 100 kV. In order to prepare the Te nanotubes decorated with Pt nanoparticles samples for TEM observations, the samples were dispersed in ethanol; then, a little amount of this ethanol dispersion was dropped onto copper grids covered by carbon layer and let to dry, slowly, in air. XPS analysis was done by using the AXIS ULTRA DLD Kratos Analytical spectrometer (Manchester, United Kingdom). The Al  $K\alpha$  (1486.6 eV) monochromatic radiation source worked at 15 kV and 15 mA. In the analysis chamber, the pressure was typically  $3 \times 10^{-9}$  torr. Widescan spectra and high resolution (HR) regions were registered in a fixed analyzer transmission (FAT) mode. The pass energy ( $E_0$ ) employed for survey regions acquisition was 160 eV, with an energy step of 1 eV, while in the HR spectra acquisition, the pass energy was of 20 eV, and energy step was 0.1 eV. The hybrid lens mode was used for all measurements with analysis area of about  $700 \mu\text{m} \times 300 \mu\text{m}$ . During the analysis, a neutralization charge system was used. Data analysis and peak fitting were done by using the software New Googly (homemade program, kindly provided by Salvi and Castle) fully described in ref. [45], that uses a self-consistent Shirley-type background officially recognized by the International Organization for Standardization (Designation: E995–16), which allows background correction, as well as curve-fitting of photoelectronic peaks. The peaks attribution, with an uncertainty on Binding Energies of  $\pm 0.1 \text{ eV}$ , was done by considering the literature data and the NIST reference database [29], and referenced to the aliphatic carbon (C1s peak signal), as an internal standard, set at 285.0 eV [26].

### 3.3. Synthesis of Tellurium Nanotubes

Large scale amounts of tellurium nanotubes were synthesized via a vapor deposition method, as reported in a previous work, and were slightly modified [27]. Powder of tellurium was positioned in a quartz boat at the middle of a tube furnace and directly evaporated onto silicon slides, as substrates ( $0.5 \times 1.0 \text{ cm}$ ) located 20 cm apart, in a constant argon gas flow (100 sccm, 99.9%). In a typical experiment, the tube was rapidly heated in 20 min from room temperature to  $400^\circ\text{C}$ , under Ar flow, and kept at this temperature for 40 min, during which the Te evaporated and deposited on the silicon substrate, spontaneously forming nanotubes. At that time, the argon gas flow was stopped and the furnace cooled naturally to the room temperature. All silicon slides used as support for the TeNTs deposition experiments, were accurately washed by ultrasonication in a mixture of water and non-ionic detergent, followed by thorough rinsing with water and ethanol to remove any remnants of the nonionic detergent, and was dried before use. Scanning electron microscope images and X-ray diffraction patterns showed that the as-synthesized Te had a nanotubular single-crystalline morphology, with a hexagonal cross-section. The Te nanotubes were typically 0.5–6 mm in length and 150–450 nm in external diameter.

### 3.4. Synthesis of Te Nanotubes Decorated with Pt Nanoparticles (TeNTs/PtNPs)

In a typical synthesis, Te nanotubes (30 mg) from previous experiments were dispersed in 20 mL of ethanol with vigorous magnetic stirring at room temperature. Then, platinum (II) chloride (10 mM) was added. The vial was capped and heated at 70 °C, under magnetic stirring, for 8 h. The TeNT/PtNP nanostructures were washed several times, in order to eliminate the excess platinum chloride and chloride that eventually did not react. The elemental composition of synthesized TeNTs/PtNPs was estimated to be 50% Pt and 50% Te (At. %), in the hypothesis that all PtCl<sub>2</sub> was reacted.

### 3.5. Preparation of the TeNTs/PtNPs/GC Modified Electrodes

Routinely, the GC electrode surfaces were polished with alumina, rinsed with deionized water and dried with N<sub>2</sub> flow. Modified electrodes were made by casting 5 µL of TeNTs/PtNPs/ethanol (8 mg/1 mL) suspension, directly onto the GC surfaces, containing about 20 µg of Pt, and left to dry at room temperature. Afterwards, TeNTs/PtNPs/GC electrodes were cycled by CV in phosphate buffer (pH 7.0, I = 0.2), starting from the measured open circuit potential (OCP), between −400 mV and +800 mV, at a scan rate of 20 mV s<sup>−1</sup>, until the current reached the steady-state conditions (typically 30 voltammetric cycles are required). The as-obtained modified electrodes were washed after this electrochemical treatment and transferred in H<sub>2</sub>SO<sub>4</sub> 0.5 M electrolyte, to be activated before their use as anodes and cathodes in a phosphate buffer (pH 7.0, I = 0.2) solution, for electrocatalytic methanol oxidation and O<sub>2</sub> reduction experiments, respectively.

## 4. Conclusions

The results of this work showed the effectiveness of TeNTs/PtNPs nanostructures for methanol electrocatalytic oxidation (MOR) and oxygen reduction (ORR), at neutral conditions suitable for fuel cell applications. The full morphological and spectroscopic characterization of TeNTs/PtNPs synthesized structures was obtained by the XRD, TEM, SAD, and XPS techniques. Results confirmed the formation of bulk structures constituted by Te nanotubes decorated with Pt nanoparticles, with a surface, enriched in average, with Pt- and Te-oxidized species, compared to platinum and tellurium bulk composition. The presence of a Pt–Te interacting species phase, confirmed by XPS, represents the sites of Pt nucleation and growth, directly grafted onto the Te nanotubes surface. The electrochemical characterization of the TeNTs/PtNPs material in aqueous electrolytic solutions at pH 7.0, was tested by cyclic voltammetry experiments. The electrocatalytic activity enhancement of the TeNTs/PtNPs structures for methanol oxidation and oxygen reduction, was proved by comparing the results with bare glassy carbon and bare platinum electrodes, as well as with the recent data reported in the literature, on systems based on both platinum and platinum-free nanostructured materials. The experiments evidence that TeNT/PtNP, opportunely activated in sulphuric acid 0.5 M solution, is a promising versatile anode/cathode electrocatalyst material for (bio)- fuel cells applications, thus, representing a valid alternative to pure platinum and platinum alloys-based electrodes, that can operate with particular efficiency in a safe neutral pH environment.

**Supplementary Materials:** The following are available online at <http://www.mdpi.com/2073-4344/9/4/328/s1>, Figure S1: Cyclic voltammetric curves on bare GC, bare Pt, and TeNT/PtNP/GC electrodes at different methanol concentrations, after subtraction of the signal in absence of methanol. Figure S2: Cyclic voltammetric curves on bare GC, bare Pt, and TeNT/PtNP/GC electrodes at O<sub>2</sub> atmospheric solution and O<sub>2</sub> saturated solutions after subtraction of the signal in absence of O<sub>2</sub>.

**Author Contributions:** Conceptualization, M.R.G. and A.T.; Methodology, F.M., M.R.G. and D.C.; Data Curation, E.F.; Writing—original draft preparation, F.M. and M.R.G. Writing—review and editing, M.R.G. and A.T.

**Funding:** This research received no external funding.

**Conflicts of Interest:** The authors declare no conflict of interest.

## References

1. Rao, C.N.R.; Kulkarni, G.U.; Thomas, P.J.; Edwards, P.P. Size-dependent chemistry: Properties of nanocrystals. *Chem. A Eur. J.* **2002**, *8*, 28–35. [[CrossRef](#)]
2. Patzke, G.R.; Krumeich, F.; Nesper, R. Oxidic nanotubes and nanorods—Anisotropic modules for a future nanotechnology. *Angew. Chem. Int. Ed.* **2002**, *41*, 2446–2461. [[CrossRef](#)]
3. Iijima, S. Helical microtubules of graphitic carbon. *Nature* **1991**, *354*, 56–58. [[CrossRef](#)]
4. Luo, X.L.; Morrin, A.; Killard, A.J.; Smyth, M.R. Application of nanoparticles in electrochemical sensors and biosensors. *Electroanalysis* **2006**, *18*, 319–326. [[CrossRef](#)]
5. Sakamoto, M.; Takamura, K. Catalytic-oxidation of biological components on platinum-electrodes modified by adsorbed metals—Anodic-oxidation of glucose. *Bioelectroch. Bioenerg.* **1982**, *9*, 571–582. [[CrossRef](#)]
6. Chen, X.L.; Pan, H.B.; Liu, H.F.; Du, M. Nonenzymatic glucose sensor based on flower-shaped au@pd core-shell nanoparticles-ionic liquids composite film modified glassy carbon electrodes. *Electrochim Acta* **2010**, *56*, 636–643. [[CrossRef](#)]
7. Toshima, N.; Yonezawa, T. Bimetallic nanoparticles—Novel materials for chemical and physical applications. *New J. Chem.* **1998**, *22*, 1179–1201. [[CrossRef](#)]
8. Liu, J.H.; Wang, A.Q.; Chi, Y.S.; Lin, H.P.; Mou, C.Y. Synergistic effect in an au-ag alloy nanocatalyst: Co oxidation. *J. Phys. Chem. B* **2005**, *109*, 40–43. [[CrossRef](#)] [[PubMed](#)]
9. Kim, M.J.; Lee, K.Y.; Jeong, G.H.; Jang, J.K.; Han, S.W. Fabrication of au-ag alloy nanoprisms with enhanced catalytic activity. *Chem. Lett.* **2007**, *36*, 1350–1351. [[CrossRef](#)]
10. Booth, M.A.; Leveneur, J.; Costa, A.S.; Kennedy, J.; Travas-Sejdic, J. Tailoring the conductivity of polypyrrole films using low-energy platinum ion implantation. *J. Phys. Chem. C* **2012**, *116*, 8236–8242. [[CrossRef](#)]
11. Jin, G.P.; Li, J.; Peng, X. Preparation of platinum nanoparticles on polyaniline-coat multi-walled carbon nanotubes for adsorptive stripping voltammetric determination of formaldehyde in aqueous solution. *J. Appl. Electrochem.* **2009**, *39*, 1889–1895. [[CrossRef](#)]
12. Shi, L.; Liang, R.P.; Qiu, J.D. Controllable deposition of platinum nanoparticles on polyaniline-functionalized carbon nanotubes. *J. Mater. Chem.* **2012**, *22*, 17196–17203. [[CrossRef](#)]
13. Xia, B.Y.; Wu, H.B.; Wang, X.; Lou, X.W. One-pot synthesis of cubic ptcu<sub>3</sub> nanocages with enhanced electrocatalytic activity for the methanol oxidation reaction. *J. Am. Chem. Soc.* **2012**, *134*, 13934–13937. [[CrossRef](#)] [[PubMed](#)]
14. Xin, Y.C.; Liu, J.G.; Zhou, Y.; Liu, W.M.; Gao, J.A.; Xie, Y.; Yin, Y.; Zou, Z.G. Preparation and characterization of pt supported on graphene with enhanced electrocatalytic activity in fuel cell. *J. Power Sources* **2011**, *196*, 1012–1018. [[CrossRef](#)]
15. Singh, R.N.; Awasthi, R.; Sharma, C.S. Review: An overview of recent development of platinum-based cathode materials for direct methanol fuel cells. *Int. J. Electrochem. Sci.* **2014**, *9*, 5607–5639.
16. Yang, L.; Ge, J.J.; Liu, C.P.; Wang, G.L.; Xing, W. Approaches to improve the performance of anode methanol oxidation reaction—a short review. *Curr. Opin. Electrochem.* **2017**, *4*, 83–88. [[CrossRef](#)]
17. Jeon, T.Y.; Lee, K.S.; Yoo, S.J.; Cho, Y.H.; Kang, S.H.; Sung, Y.E. Effect of surface segregation on the methanol oxidation reaction in carbon-supported pt-ru alloy nanoparticles. *Langmuir* **2010**, *26*, 9123–9129. [[CrossRef](#)]
18. He, C.; Desai, S.; Brown, G.; Bollepalli, S. *PEM Fuel Cell Catalysts: Cost, Performance, and Durability*; The Electrochemical Society Interface: Pennington, NJ, USA, 2005; pp. 41–44.
19. Ding, Y.M.; Liu, Y.L.; Rao, G.S.; Wang, G.F.; Zhong, Q.L.; Ren, B.; Tian, Z.Q. Electrooxidation mechanism of methanol at pt-ru catalyst modified gc electrode in electrolytes with different ph using electrochemical and sers techniques. *Chin. J. Chem.* **2007**, *25*, 1617–1621. [[CrossRef](#)]
20. Yan, B.; Concannon, N.M.; Milshtein, J.D.; Brushett, F.R.; Surendranath, Y. A membrane-free neutral ph formate fuel cell enabled by a selective nickel sulfide oxygen reduction catalyst. *Angew. Chem. Int. Ed.* **2017**, *56*, 7496–7499. [[CrossRef](#)]
21. Tominaka, S.; Nishizeko, H.; Ohta, S.; Osaka, T. On-chip fuel cells for safe and high-power operation: Investigation of alcohol fuel solutions. *Energy Environ. Sci.* **2009**, *2*, 849–852. [[CrossRef](#)]
22. Lehmann, K.; Yurchenko, O.; Urban, G. Carbon nanowalls for oxygen reduction reaction in bio fuel cells. *J. Phys. Conf. Ser.* **2014**, *557*, 012008. [[CrossRef](#)]
23. Santoro, C.; Arbizzani, C.; Erable, B.; Ieropoulos, I. Microbial fuel cells: From fundamentals to applications. A review. *J. Power Sources* **2017**, *356*, 225–244. [[CrossRef](#)]

24. Huang, M.H.; Wang, F.; Li, L.R.; Guo, Y.L. A novel binary pt<sub>3</sub>tex/c nanocatalyst for ethanol electro-oxidation. *J. Power Sources* **2008**, *178*, 48–52. [CrossRef]
25. Guascito, M.R.; Chirizzi, D.; Malitesta, C.; Siciliano, M.; Siciliano, T.; Tepore, A. Amperometric non-enzymatic bimetallic glucose sensor based on platinum tellurium microtubes modified electrode. *Electrochem. Commun.* **2012**, *22*, 45–48. [CrossRef]
26. Guascito, M.R.; Chirizzi, D.; Malitesta, C.; Siciliano, T.; Tepore, A. Te oxide nanowires as advanced materials for amperometric nonenzymatic hydrogen peroxide sensing. *Talanta* **2013**, *115*, 863–869. [CrossRef]
27. Siciliano, T.; Filippo, E.; Genga, A.; Micocci, G.; Siciliano, M.; Tepore, A. Single-crystalline te microtubes: Synthesis and no(2) gas sensor application. *Sens. Actuators B Chem.* **2009**, *142*, 185–190. [CrossRef]
28. Guascito, M.R.; Chirizzi, D.; Malitesta, C.; Mazzotta, E.; Siciliano, M.; Siciliano, T.; Tepore, A.; Turco, A. Low-potential sensitive H<sub>2</sub>O<sub>2</sub> detection based on composite micro tubular te adsorbed on platinum electrode. *Biosens. Bioelectron.* **2011**, *26*, 3562–3569. [CrossRef] [PubMed]
29. Nist X-Ray Photoelectron Spectroscopy Database. Available online: <https://srdata.nist.gov/xps/Default.aspx> (accessed on 16 January 2019).
30. Mayers, B.; Jiang, X.C.; Sunderland, D.; Cattle, B.; Xia, Y.N. Hollow nanostructures of platinum with controllable dimensions can be synthesized by templating against selenium nanowires and colloids. *J. Am. Chem. Soc.* **2003**, *125*, 13364–13365. [CrossRef]
31. Bard, A.J.; Faulkner, L.R. *Electrochemical Methods: Fundamentals and Applications*, 2nd ed.; Wiley: New York, NY, USA, 2000.
32. Chen, X.M.; Tian, X.T.; Zhao, L.M.; Huang, Z.Y.; Oyama, M. Nonenzymatic sensing of glucose at neutral ph values using a glassy carbon electrode modified with graphene nanosheets and pt-pd bimetallic nanocubes. *Microchim. Acta* **2014**, *181*, 783–789. [CrossRef]
33. Ernst, S.; Heitbaum, J.; Hamann, C.H. The electrooxidation of glucose in phosphate buffer solutions: Part i. Reactivity and kinetics below 350 mv/rhe. *J. Electroanal. Chem. Interfacial Electrochem.* **1979**, *100*, 173–183. [CrossRef]
34. Park, S.; Boo, H.; Chung, T.D. Electrochemical non-enzymatic glucose sensors. *Anal. Chim. Acta* **2006**, *556*, 46–57. [CrossRef]
35. Kadirgan, F.; Beden, B.; Leger, J.M.; Lamy, C. Synergistic effect in the electrocatalytic oxidation of methanol on platinum+palladium alloy electrodes. *J. Electroanal. Chem. Interfacial Electrochem.* **1981**, *125*, 89–103. [CrossRef]
36. Filippo, E.; Baldassarre, F.; Tepore, M.; Guascito, M.R.; Chirizzi, D.; Tepore, A. Characterization of hierarchical alpha-moo<sub>3</sub> plates toward resistive heating synthesis: Electrochemical activity of alpha-moo<sub>3</sub>/pt modified electrode toward methanol oxidation at neutral ph. *Nanotechnology* **2017**, *28*, 215601. [CrossRef] [PubMed]
37. Rosenbaum, M.; Schroder, U.; Scholz, F. Investigation of the electrocatalytic oxidation of formate and ethanol at platinum black under microbial fuel cell conditions. *J. Solid State Electr.* **2006**, *10*, 872–878. [CrossRef]
38. Sadhukhan, M.; Kundu, M.K.; Bhowmik, T.; Barman, S. Highly dispersed platinum nanoparticles on graphitic carbon nitride: A highly active and durable electrocatalyst for oxidation of methanol, formic acid and formaldehyde. *Int. J. Hydrog. Energy* **2017**, *42*, 9371–9383. [CrossRef]
39. Jing, S.C.; Guo, X.L.; Tan, Y.W. Branched pd and pd-based trimetallic nanocrystals with highly open structures for methanol electrooxidation. *J. Mater. Chem. A* **2016**, *4*, 7950–7961. [CrossRef]
40. Li, H.H.; Zhao, S.; Gong, M.; Cui, C.H.; He, D.; Liang, H.W.; Wu, L.; Yu, S.H. Ultrathin ptpdte nanowires as superior catalysts for methanol electrooxidation. *Angew. Chem. Int. Ed.* **2013**, *52*, 7472–7476. [CrossRef] [PubMed]
41. Xu, J.; Wang, Z.H.; Li, H.H.; Liu, J.W.; Yu, S.H. Templating synthesis of ternary ptpdte nanowires with tunable diameter for methanol electrooxidation. *CrystEngComm* **2016**, *18*, 4038–4041. [CrossRef]
42. Nguyen, M.T.; Mecheri, B.; Iannaci, A.; D'Epifanio, A.; Licocchia, S. Iron/polyindole-based electrocatalysts to enhance oxygen reduction in microbial fuel cells. *Electrochim. Acta* **2016**, *190*, 388–395. [CrossRef]
43. Jin, Y.D.; Shen, Y.; Dong, S.J. Electrochemical design of ultrathin platinum-coated gold nanoparticle monolayer films as a novel nanostructured electrocatalyst for oxygen reduction. *J. Phys. Chem. B* **2004**, *108*, 8142–8147. [CrossRef]

44. Zhong, H.X.; Zhang, H.M.; Liang, Y.M.; Zhang, J.L.; Wang, M.R.; Wang, X.L. A novel non-noble electrocatalyst for oxygen reduction in proton exchange membrane fuel cells. *J. Power Sources* **2007**, *164*, 572–577. [[CrossRef](#)]
45. Salvi, A.M.; Castle, J.E. The intrinsic asymmetry of photoelectron peaks: dependence on chemical state and role in curve fitting. *J. Electron. Spectros. Relat. Phenomena* **1998**, *95*, 45–56. [[CrossRef](#)]



© 2019 by the authors. Licensee MDPI, Basel, Switzerland. This article is an open access article distributed under the terms and conditions of the Creative Commons Attribution (CC BY) license (<http://creativecommons.org/licenses/by/4.0/>).